Chemical Engineering Research and Design 223 (2025) 30–44

Contents lists available at ScienceDirect

Chemical Engineering Research and Design

journal homepage: www.elsevier.com/locate/cherd

Kinetic model identification for hydrogen borrowing synthesis using a cloud platform for model-based design of experiments

Emmanuel Agunloye [a], Ricardo Labes [b], Thomas Chamberlain [b], Frans L. Muller [b], Richard A. Bourne [b], Federico Galvanin [a,*]

[a] Department of Chemical Engineering, University College London, London WC1E 7JE, United Kingdom
[b] School of Chemical and Process Engineering, University of Leeds, Leeds LS2 9JT, United Kingdom

ARTICLE INFO

Keywords:
Hydrogen borrowing
Kinetics modeling
Model-based design of experiments
Model discrimination
Sequential parameter estimation

ABSTRACT

Hydrogen borrowing is an increasingly important catalytic process in the synthesis of pharmaceutical intermediates and active drug compounds. Its mechanism is typically described as a three-step sequence: alcohol oxidation, additive alkylation (or arylation) and hydrogen reduction. While the mechanistic steps are well established, the development of predictive kinetic models is critical to enabling process scalability and automation. In this work, the hydrogen borrowing mechanism is embedded within a model-based design of experiments (MBDoE) framework for controlling automated laboratory experimentation via a cloud service. A case study involving benzyl alcohol and benzylamine reaction over a Ru catalyst was conducted. Candidate kinetic models were developed to describe the dynamics of reactants, intermediates and products based on experimental data. Leveraging MBDoE in combination with a novel sequential parameter estimation technique informed by the reaction network, two statistically adequate and identifiable kinetic models were identified. Although initially indistinguishable based on standard experimental data, in-silico simulations exploiting structural differences between the models show that catalyst amount acts as a key model discrimination factor. This work demonstrates how reaction-informed model discrimination through targeted experimental design can advance understanding and control of hydrogen borrowing synthesis, laying the foundation for more robust and scalable processes in the pharmaceutical industry.

1. Introduction

Many pharmaceutical companies still rely on batch manufacturing and traditional technologies, such as basic sensors and analog instruments (Powner and Yalcinkaya, 1995; Lee et al., 2015; Wichrowski et al., 2020; Rossi, 2022; NASEM National Academies of Sciences, Engineering, and Medicine, 2024; Kaylor, 2025). While these technologies have been reliable over the years, they pose challenges for scalability and consistent quality assurance – especially as global demand for medicines continues to grow. Between 2018 and 2021, hundreds of drugs were recalled annually due to quality-related issues, highlighting the significant health and economic consequences of current limitations (Destro and Barolo, 2022). In response, industry experts and regulatory bodies have strongly advocated for the implementation of industry 4.0 technologies within the pharmaceutical sector. These include robotics, artificial intelligence (AI), cloud computing, digitalization, continuous manufacturing and process analytics technologies (PAT), Collectively, these technologies are positioned to modernize pharmaceutical manufacturing and address long-standing challenges in process efficiency and product quality (Yu et al., 2019; Fisher et al., 2019). Indeed, many of these technologies and their implementations rely on mathematical modeling to support real-time control, optimization and process design (Destro and Barolo, 2022; Chatterjee et al., 2017). These models are typically developed following two broad approaches: (1) data-driven, and (2) physics-based. While data-driven approaches offer faster development and greater computational efficiency, physics-based models provide deeper process understanding, improved robustness and better extrapolation capabilities. Moreover, they align more closely with the pharmaceutical industry's quality-by-design (QbD) principles (Yu et al., 2014), supporting regulatory compliance and systematic process control.

By applying mathematical models, one can define and explore the design space of pharmaceutical processes – the range of operating conditions under which product quality can be assured – an essential component of QbD. Beyond regulatory compliance, this design space

* Corresponding author.
E-mail address: f.galvanin@ucl.ac.uk (F. Galvanin).

https://doi.org/10.1016/j.cherd.2025.09.005
Received 8 April 2025; Received in revised form 28 July 2025; Accepted 3 September 2025
Available online 13 September 2025

Nomenclature

Scalars

c_i i^{th}	Species concentration
$E_{a,j}$	Activation energy of reaction j
$J_{i,j}$	Model prediction divergences
$J_{1,2,3,\ldots}$	Joint divergence
k_j	Kinetic rate constant for j^{th} reaction
$k_{j,ref}$	Rate constant of reaction j at T_{ref}
N_s	Total number of samples
N_m	Number of models
p^i	Probability density function for model i
r_j	Reaction rate (mol/s.L) for the j^{th} reaction
R	Universal gas constant equal to 8.31 $\frac{kJ}{mol.K}$
T	Reactor temperature
ν_{ij}	Stoichiometric coefficient
τ	Space time
κ	Condition number
χ^2	Chi-square statistic

Vectors

$\mathbf{c}\in N^{n_c}$	Vector of the state variables (concentrations)
$\mathbf{H}$	Fisher information matrix corresponds
$\mathbf{u}\in N^{n_u}$	Vector of manipulated variables
$\mathbf{U}$	Unitary matrix whose columns are the normalized eigenvectors of $\mathbf{H}$
$\boldsymbol{x}\in\mathbb{R}^{N_x}$	Vector of state variables
$\dot{x}$	First derivative of the state variables
$\widehat{\boldsymbol{y}}\in\mathbb{R}^{N_y}$	Vector of model predictions for measurements $\boldsymbol{y}$
$\boldsymbol{\theta}\in N^{n_\theta}$	Vector of the kinetic parameters to be identified
$\sum_0$	Preliminary variance-covariance matrix of model parameters
$\sum_y$	Measurement error covariance matrix
Λ	Diagonal matrix of the eigenvalues
$\sum_i$	Covariance matrix for model i predictions

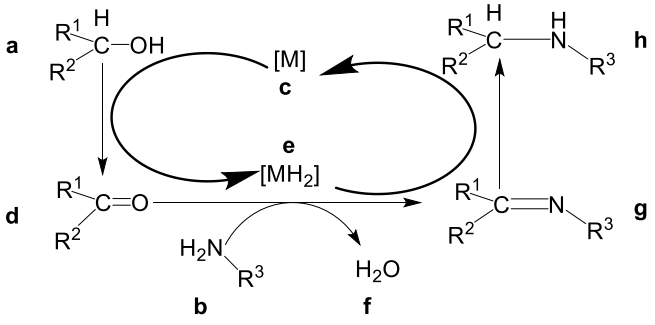

Fig. 1. Hydrogen borrowing reaction scheme with 3 elementary chemical steps involving chemical species {a}, {b} and {c} as starting materials; {d}, {e}, and {g} as intermediate species; {c}, {f} and {h} as final products (Reed-Berendt et al., 2021).

can also be optimized for economic performance using design of experiments (DoE) methodologies (Chatterjee et al., 2017; Collins, 2018). Traditional DoE techniques, such as factorial designs (Box and Draper, 1987; Yuangyai et al., 2010), and randomized experiments (Caliński and Kageyama, 2000), are widely used. However, when a mechanistic model is available, more targeted experimental design is possible through model-based design of experiments (MBDoE) (Franceschini and Macchietto, 2008). MBDoE leverages the underlying process model to design optimal experiments that yield maximally informative data, enabling accurate parameter estimation (Franceschini and Macchietto, 2008), or/and 2) model discrimination (Waldron et al., 2019). Using physics-based models, MBDoE can tailor experimental campaigns to fit available resources while improving model performance in terms of both parameter uncertainty and predictive capability (Franceschini and Macchietto, 2008). To be effective MBDoE requires not only robust models but also efficient parameter estimation algorithms and experimental scheduling systems. Our recent publication demonstrated the application of online MBDoE techniques to automate a cloud-based experimental platform, executing a sequence of optimal steady-state experiments in a smart flow reactor (Agunloye et al., 2024). This platform integrates the experimental subsystem, known as the LabBot, with a software subsystem called the SimBot, which houses the MBDoE algorithms used for kinetic model identification. Together, the LabBot-SimBot system enables automated experimentation informed by real-time model analysis, demonstrating a novel approach to accelerating pharmaceutical process development.

In this study, we apply this cloud-based MBDoE platform to a hydrogen borrowing reaction system. Hydrogen borrowing is an emerging synthetic methodology under exploration by the pharmaceutical industry for new drug discovery (Leonard et al., 2015; Reed-Berendt et al., 2021). While historically many drugs were isolated from natural sources, today's pharmaceutical compounds are predominantly produced via multi-step organic syntheses from precursors such as alcohols, amines, amides and esters (Karimi et al., 2015; Kent et al., 2016). These synthesis frequently involve alkylation and arylation reactions – transformations well-suited to the hydrogen borrowing strategy. Hydrogen borrowing enables such transformations via a flexible catalytic cycle consisting of: (1) alcohol oxidation, (2) nucleophilic substitution (e.g., alkylation or arylation), and (3) hydrogen transfer (reduction). This mechanism supports chain elongation and ring construction and is therefore valuable in expanding chemical diversity in drug candidates (Reed-Berendt et al., 2021). Because the mechanism can be described through a well-established kinetic framework (e.g., based on Arrhenius expressions), it is ideally suited for physics-based modeling and MBDoE-based experimentation.

In this study, we supplement the standard MBDoE workflow with a sequential parameter estimation technique, tailored to the hydrogen borrowing reaction network. This enhancement improves the numerical solution of parameter estimation and model discrimination under conditions of limited data – crucial for developing an autonomous, cloud-controlled laboratory platform.

This paper presents a comprehensive study of kinetic model identification for hydrogen borrowing synthesis using the LabBot-SimBot platform. Section 2 introduces the chemical reactions and experimental setup within the LabBot. Section 3 details the modeling framework and parameter estimation procedures implemented in the SimBot. Section 4 presents and discusses the application of MBDoE for kinetic model identification and discrimination. Section 5 concludes with implications for process development and automation in pharmaceutical research.

2. Hydrogen borrowing chemical synthesis

Hydrogen borrowing is a widely used catalytic reaction for increasing molecular complexity in organic compounds bearing alcohol functionalities (Reed-Berendt et al., 2021). The reaction occurs when three substances are present: an alcohol {a}, an amine {b}, and a metal catalyst {c}, reacting in three steps. In the first step, the metal oxidizes

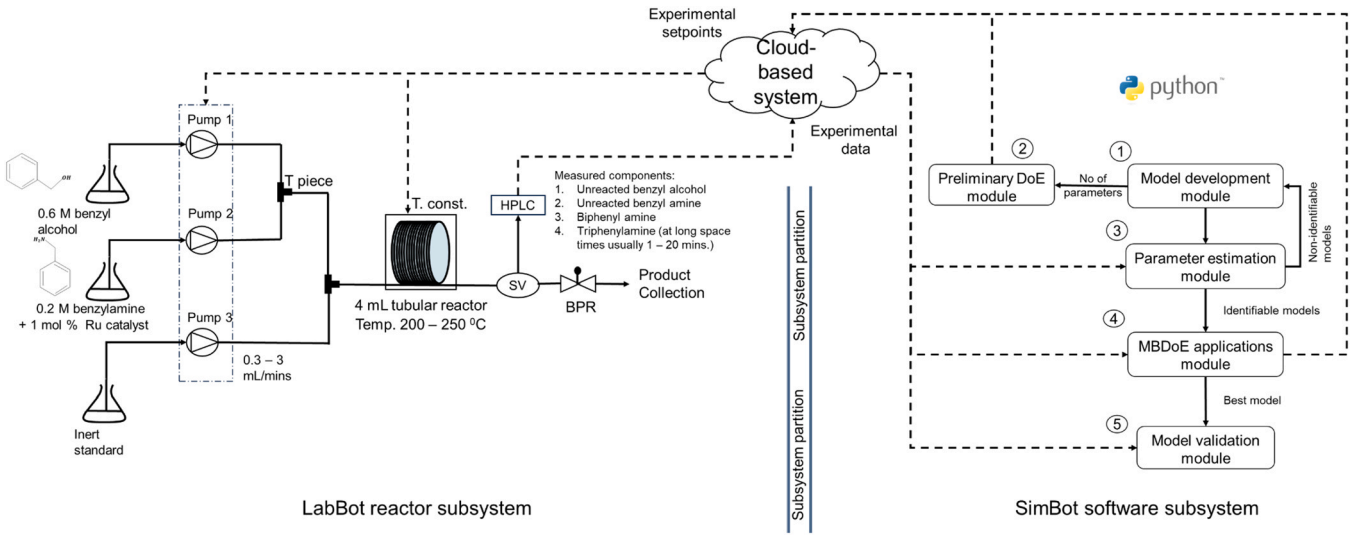

Fig. 2. Schematic of the cloud-based approach comprising the LabBot subsystem, a physical, automated experimental setup composed of various enabling equipment and the SimBot subsystem comprising 5 modules implemented in Python and integrated with the cloud services for data access and setpoints specification.

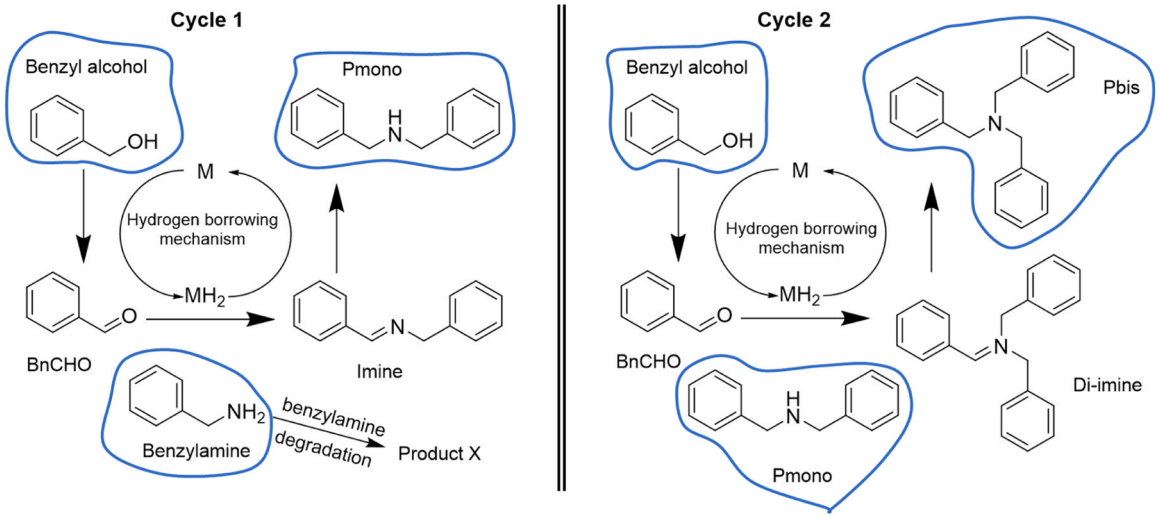

Fig. 3. Scheme to describe the formation of measured species from the starting reactants based on hydrogen borrowing.

the alcohol to its aldehyde {d} by borrowing hydrogen (metal hydride {e}). In the second step, the aldehyde combines with the amine, which acts as a nucleophile, to form intermediate {g} and a by-product {f}. In the third step, the metal catalyst releases the borrowed hydrogen to convert the intermediate to a stable product {h}. Fig. 1 shows the hydrogen borrowing reaction scheme.

The reaction was carried out in the LabBot reactor subsystem, a smart flow experimental setup controlled remotely via a cloud system using the SimBot software subsystem. The LabBot subsystem includes 3 pumps, 2 tee-pieces, a tubular reactor coil, a sampling valve (SV) and a back-pressure regulator (BPR). The sampling valve was used to send a sample for high performance liquid chromatography (HPLC) for online analysis. Fig. 2 shows the LabBot and SimBot subsystems and their interactions within the cloud-based system. Further details about the LabBot automation can be found in a recent publication (Agunloye et al., 2024) while the SimBot modules relevant to the hydrogen borrowing study will be discussed in Section 3. The LabBot operating ranges for the various pieces of equipment were set, with pumps calibrated to operate between 0.3 and 3 mL/mins, and the reactor temperature controlled within the range of 200 – 250 ^{0}C. The stock concentrations of the specific reactants used in this study - benzyl alcohol (0.6 M), and benzyl amine (0.2 M)) - were selected to ensure that both reactants and products could be accurately measured over the range of the conditions explored. Note that the stock concentrations differ from the reactor inlet concentrations flowing from the second tee-piece. The metal catalyst was fixed at 1 mol% of the amine to reduce the number of pumps required, allowing a wider window of reactant ratios to be explored. An inert internal standard was used to calibrate reactants' concentrations in the HPLC, enabling accurate measurement of unreacted benzyl alcohol, unreacted benzyl amine, biphenylamine, and triphenylamine (at long space times). Note that the catalyst is in homogeneous solution with the reactants (Huang et al., 2021).

Based on the measurements presented later in Section 4, the synthesis can be explained using two cycles of the hydrogen borrowing scheme as illustrated in Fig. 3. In Cycle 1, the metal first oxidizes benzyl alcohol to benzyl aldehyde by borrowing hydrogen. Then, benzyl aldehyde combines with benzylamine to form unstable biphenyl imine, which on reaction with the borrowed hydrogen reduces to biphenyl amine. Cycle 2 produces triphenylamine by combining biphenylamine with benzylaldehyde to form unstable triphenyl imine that reduces on reacting with borrowed hydrogen. While Cycle 1 consumes both benzyl alcohol and benzyl amine in a molar ratio of 1:1, Cycle 2 consumes

Table 1
A breakdown of the six derived models for the scheme in Fig. 3 with their components, chemical steps and rate equations.

	Model 1	Model 2	Model 3	Model 4	Model 5	Model 6
Step 1	$BnOH \xrightarrow{r_1} BnCHO$	$BnOH + Me \xrightarrow{r_1} BnCHO + MeH_2$	$BnOH + Me \xrightarrow{r_1} BnCHO + MeH_2$	$BnOH + Me \xrightarrow{r_1} BnCHO + MeH_2$	$BnOH + Me \xrightarrow{r_1} BnCHO + MeH_2$	$BnOH + Me \xrightarrow{r_1} BnCHO + MeH_2$
Step 2	$BnCHO + BnNH_2 \xrightarrow{r_2} Pmono$	$BnCHO + BnNH_2 \xrightarrow{r_2} Pmono$	$BnCHO + BnNH_2 \xrightarrow{r_2} Pmono$	$BnCHO + BnNH_2 \xrightarrow{r_2} Imine$	$BnCHO + BnNH_2 \xrightarrow{r_2} Imine + H_2O$	$BnCHO + BnNH_2 \xrightarrow{r_2} Imine + H_2O$
Step 3	$BnNH_2 \xrightarrow{r_3} Product\ X$	$BnNH_2 \xrightarrow{r_3} Product\ X$	$BnCHO + Pmono \xrightarrow{r_3} Pbis$	$Imine + MeH_2 \xrightarrow{r_3} Pmono$	$Imine + MeH_2 \xrightarrow{r_3} Pmono$	$Imine + MeH_2 \xrightarrow{r_3} Pmono$
Step 4			$BnNH_2 \xrightarrow{r_4} Product\ X$	$BnCHO + Pmono \xrightarrow{r_4} Pbis$	$BnCHO + Pmono \xrightarrow{r_4} Pbis$	$BnCHO + Pmono \xrightarrow{r_4} Di - imine + H_2O$
Step 5				$BnNH_2 \xrightarrow{r_5} Product\ X$	$BnNH_2 \xrightarrow{r_5} Product\ X$	$Diimine + H_2 \xrightarrow{r_5} Pbis$
Step 6						$BnNH_2 \xrightarrow{r_6} Product\ X$
Number of components	5	7	8	9	10	11
Rate equations	$r_1 = k_1c_1$ $r_2 = k_2c_2c_3$ $r_3 = k_3c_3$	$r_1 = k_1c_1c_6$ $r_2 = k_2c_2c_3$ $r_3 = k_3c_3$	$r_1 = k_1c_1c_6$ $r_2 = k_2c_2c_3$ $r_3 = k_3c_2c_4$ $r_4 = k_4c_3$	$r_1 = k_1c_1c_6$ $r_2 = k_2c_2c_3$ $r_3 = k_3c_9$ $r_4 = k_4c_2c_4$ $r_5 = k_5c_3$	$r_1 = k_1c_1c_6$ $r_2 = k_2c_2c_3$ $r_3 = k_2c_9$ $r_4 = k_2c_2c_4$ $r_5 = k_5c_3$	$r_1 = k_1c_1c_6$ $r_2 = k_2c_2c_3$ $r_3 = k_3c_7c_9$ $r_4 = k_4c_2c_4$ $r_5 = k_5c_6c_{10}$ $r_6 = k_6c_3$
Chemical species	$c_1 = BnOH$, $c_2 = BnCHO$, $c_3 = BnNH_2$, $c_4 = Pmono$, $c_5 = X$	$+ c_6 = Me$, $c_7 = MH_2$	$+ c_8 = Pbis$	$+ c_9 = Imine$	$+ c_{10} = H_2O$	$+ c_{11} = Di - imine$

benzyl alcohol and biphenyl amine in the same ratio of 1:1 when it occurs. The complete hydrogen borrowing reaction would therefore require a stoichiometric ratio of 2:1 benzyl alcohol to benzyl amine. However, the inlet concentration ratios for most of the synthesis experiments were less than two, as presented in Section 4 with benzylamine inlet concentration fixed at 0.1 M while that of benzyl alcohol changing from 0.054 to 0.231 M. Thus, in the synthesis, conversion is defined as the fraction of reacted benzyl alcohol compared to the inlet concentration as this is limiting reactant and should be equal or greater than the amount of benzyl amine when present in stoichiometric amounts. However, the measurements consistently showed that the reverse was the case: benzyl amine conversion was greater than benzyl alcohol. To explain these measurements, we assumed that benzyl amine converts via a side reaction. Fig. 3 shows the scheme of reactions applicable in this case study. In Section 4, we report the results from this scheme and from that, not considering the side reaction in Appendix 1 in the electronic supplementary information (ESI). In the following section, we derive models for this reaction scheme and we detail the procedure for model identification.

3. Section 3: Model development and identification procedure

The LabBot subsystem for hydrogen borrowing presented in the previous section generated experimental data and exchanged communication via the cloud with the Simbot subsystem, the software that generated the experimental setpoints. The Simbot software implemented in Python programming language as illustrated by Fig. 2 comprises 5 modules: model development, preliminary design of experiment (DoE), parameter estimation, model-based design of experiment (MBDoE) applications and model validation. Further details about the communication protocol between the LabBot and SimBot can be found in our recent publication (Agunloye et al., 2024).

3.1. Model development module

For model development, we employed material balance equations to describe the evolution of each chemical components influenced by the various chemical reactions in the LabBot plug flow reactor. We describe the plug flow reactor system operating at steady state as:

$$\frac{dc_i}{d\tau} = -\sum_{j=1}^{N^r} \nu_{ij} r_j \tag{1}$$

where c_i is the i^{th} species concentration, r_j is the reaction rate ($mols^{-1}\ L^{-1}$) of the j^{th} reaction with the ν_{ij} the stoichiometric coefficient, respectively and τ is the space time. To express r_j and ν_{ij}, we need balanced chemical equations of the various mechanistic steps reported in Fig. 3. This introduces new intermediate chemical species outside the measured components. The measured components are benzyl alcohol, benzylamine and diphenylamine, while intermediates are involved in the first and second hydrogen borrowing cycles. Table 1 shows a breakdown of six potential kinetic models derived from Fig. 3, each with increasing complexity:(1) Model 1 accounts for 5 components in 3 chemical steps; (2) Model 2 accounts for 7 components in 3 chemical steps; (3) Model 3 accounts for 8 components in 4 chemical steps; (4) Model 4 accounts for 9 components in 5 chemical steps; (5) Model 5 accounts for 10 components; (6) and lastly Model 6 accounts for 11 components in 6 chemical steps, to describe the scheme completely.

The rate in the j-th reaction has been expressed according to a power law model as:

$$r_j = k_j c_i c_k \tag{2}$$

where c_i is the i^{th} species concentration, and k_j the reaction rate constant whose temperature dependence is given by the Arrhenius equation, written in a reparametrized form as (Schwaab et al., 2008):

$$k_j = k_{j,ref} e^{\left[-\frac{E_{a,j}}{R}\left(\frac{1}{T}-\frac{1}{T_{ref}}\right)\right]} \tag{3}$$

$k_{j,ref}$ is the rate constant of reaction j at T_{ref}, $E_{a,j}$ is the activation energy of reaction j, T is the reactor temperature, R is the universal gas constant equal to $8.31 \frac{kJ}{mol.K}$. Parameters $k_{j,ref}$ and $E_{a,j}$ are calculated using parameter estimation.

The models obtained by coupling the reactor model in Eq. (1) and the rate equations in Eq. (2) are expressed in terms of differential and algebraic equations (DAEs) generally written as:

$$\mathbf{f}\left(\frac{d\mathbf{c}}{d\tau}(\tau), \mathbf{c}(\tau), \mathbf{u}(\tau), \boldsymbol{\theta}, \tau\right) = 0,\ with\ \mathbf{c}(0) = \mathbf{c}_0 \tag{4}$$

Table 2
Experimental design space of control variables employed in the hydrogen borrowing case study of benzylamine and benzyl alcohol.

Limits	$c_1(0)$ (M)	$c_2(0)$ (M)	τ(min)	$Temp(^{\circ}C)$
Lower	0.100	0.050	1.0	200
Upper	0.100	0.250	15.0	250

with $\mathbf{c} \in N^{n_c}$ being the vector of the state variables (concentrations of the chemical species in this case), $\mathbf{u} \in N^{n_u}$ being the vector of manipulated variables (reactants' inlet concentrations, and reactor temperature), $\boldsymbol{\theta} \in N^{n_\theta}$ being the vector of the kinetic parameters to be identified, $\boldsymbol{\theta} = [\ldots, k_{j,ref}, E_{a,j}, \ldots]$.

3.2. Parameter estimation module

Developed models comprise nonlinear equations describing sequential and coupled chemical steps and can be a reliable representation of the chemical system if parameters are estimated precisely. Bard discussed the standard approach for nonlinear parameter estimation of a full parameter set from experimental data (Bard, 1974). Nonlinear models for sequential and coupled chemical steps pose another problem: high parameter correlation. Past authors including Yue et al., Srinath and Gunawan, and Thomson et al. decorrelated the parameters focusing on a parameter subset judged based on available data (Yue et al., 2006; Srinath and Gunawan, 2010; Thompson et al., 2010). This strategy has been formalized into various algorithms for decorrelating the model parameters using the Fisher information matrix (Franceschini and Macchietto, 2008). In this work, we present a sequential parameter estimation (SPE) technique that is informed by the measurements and the developed kinetic models for the hydrogen borrowing reaction. We apply the SPE by first selecting an identifiable parameter subset for preliminary estimation and then fixing this subset of parameters to improve the estimation of the remaining parameters. We discuss the standard and sequential parameter estimation approaches in the following sections.

3.2.1. Standard nonlinear parameter estimation

Model parameters can be estimated via nonlinear optimization by fitting the model to experimental measurements, which comprise random experimental error. To account for the random nature of the error of experimental measurements, the objective function for parameter estimation (PE) is defined using the likelihood function and optimized by minimizing the negative log-likelihood (Bard, 1974):

$$obj = \min_{\boldsymbol{\theta}} \left[\log(2\pi)^{N_s N_y} + \sum_{s=1}^{N_s} \sum_{k=1}^{N_y} \log\det \boldsymbol{V}_{\boldsymbol{y}} + (\widehat{\boldsymbol{y}} - \boldsymbol{y})^T \boldsymbol{\Sigma}_{\boldsymbol{y}}^{-1} (\widehat{\boldsymbol{y}} - \boldsymbol{y}) \right] \quad (5)$$

subject to the model equations and the state space constraints:

$$\boldsymbol{f}(\dot{\boldsymbol{x}}(\tau), \boldsymbol{x}(\tau), \quad \boldsymbol{u}(\tau), \boldsymbol{\theta}, \tau) = \mathbf{0} \quad (6)$$

$$\widehat{\boldsymbol{y}}(\tau) = \boldsymbol{g}(\boldsymbol{x}(\tau)) \quad (7)$$

$$\boldsymbol{x}(0) = \boldsymbol{x}_0 \quad (8)$$

$$\boldsymbol{\varphi} = \left[\boldsymbol{u}^T, \tau, \boldsymbol{x}_0{}^T \right]^T \quad (9)$$

$$\boldsymbol{x}(\tau) \in \mathscr{X} \quad (10)$$

where $\boldsymbol{x} \in \mathbb{R}^{N_x}$ is the vector of state variables; $\dot{\boldsymbol{x}}$ is the first derivative of the state variables; $\boldsymbol{u} \in \mathbb{R}^{N_u}$ is the vector of inputs or control variables that define the condition of an experiment; $\boldsymbol{\theta} \in \mathbb{R}^{N_\theta}$ is the vector of model parameters; $\widehat{\boldsymbol{y}} \in \mathbb{R}^{N_y}$ is the vector of model predictions for measurements $\boldsymbol{y}$; $\boldsymbol{\Sigma}_{\boldsymbol{y}}$ is the measurement error covariance matrix; and N_s is the total number of samples. Eq. (6) gives the differential equations resulting from the material balance on the components, while Eq. (7) gives the algebraic equations relating measurements to the state variables. Eqs. (8) and (9) define the initial conditions and experimental design vector, respectively, with the state variables being in the state space as illustrated in (10).

The resulting problem is an optimization problem which requires two steps: integration of the DAEs and constrained nonlinear optimization of Eq. (5). DAEs can be integrated symbolically using the orthogonal collocation method reported in the work of Biegler (2010) and implemented in the CasADi (an acronym for Computer algebra systems for Algorithmic Differentiation) Python library (Andersson et al., 2019; CasADi, 2024) to obtain a set of algebraic equations (Bynum et al., 2021) that are solved using IPOPT (an acronym for Interior Point OPTimizer), an algorithm for large-scale nonlinear optimization of continuous systems (Wächter and Biegler, 2006; AGI Ansys Government Initiative, 2024). IPOPT evaluates the set of parameter values $\widehat{\boldsymbol{\theta}}$ that minimizes the Lagrangian function of the negative log-likelihood variable term and the resulting algebraic equations. The resulting Lagrangian expression can, however, prohibit the optimization algorithm from achieving a unique solution in the full parameter estimation, some parameters exhibiting high correlation thereby making the model practically non-identifiable (Shahmohammadi and McAuley, 2019).

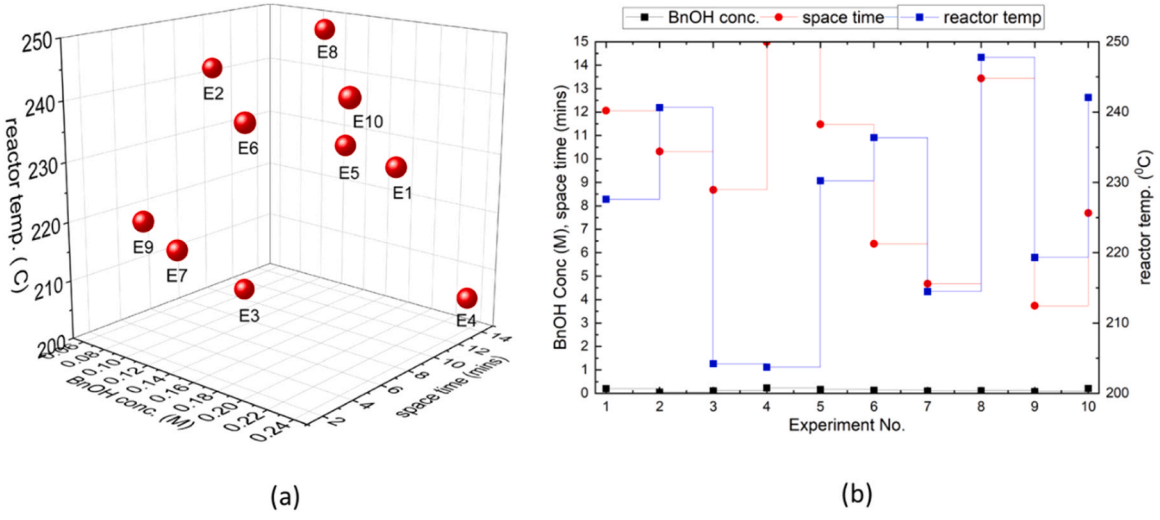

Fig. 4. 10 preliminary experiments with 3 control variables of BnOH conc, space time and reactor temperature designed using the Latin hypercube sampling while keeping BnNH constant at 0.1 M: in the experimental design space (a) and the corresponding experimental trajectory (b).

Table 3
Outlet measurements from the LabBot system and the corresponding performance of the synthesis at each synthesis condition using reactants conversions, and product yields: diphenylamine (Pmono) and triphenylamine (Pbis). Max and min values in each column are indicated in green and red, respectively. The LabBot system reported zero for PBis outlet concentrations in these 10 experiments.

	Inlet conditions				Outlet conditions						
Exp No	Temp (°C)	res time (mins)	BnNH (M)	BnOH (M)	BnNH (M)	BnOH (M)	Pmono (M)	Pbis (M)	OH conversion (%)	NH conversion (%)	Pmono yield (%)
1	227.603	12.055	0.100	0.1978	0.0690	0.1760	0.0073	0	11.046	31.181	23.200
2	240.636	10.317	0.100	**0.0546**	0.0624	**0.0480**	0.0063	0	12.078	37.739	16.689
3	204.214	8.679	0.100	0.1051	0.0767	0.0988	**0.0018**	0	6.008	23.536	**7.621**
4	**203.720**	**14.982**	0.100	**0.2309**	0.0752	**0.2171**	0.0036	0	5.995	25.065	14.246
5	230.240	11.471	0.100	0.1615	0.0674	0.1460	0.0070	0	9.582	32.788	21.226
6	236.360	6.377	0.100	0.1362	0.0684	0.1245	0.0056	0	8.634	31.783	17.424
7	214.463	4.675	0.100	0.0972	0.0792	0.0920	0.0022	0	5.369	21.019	10.205
8	**247.791**	13.439	0.100	0.1201	**0.0605**	0.0839	**0.0096**	0	**30.110**	**39.654**	24.258
9	219.322	**3.735**	0.100	0.0797	**0.0815**	0.0770	0.0022	0	**3.342**	**18.723**	11.925
10	242.078	7.688	0.100	0.2060	0.0708	0.1692	0.0088	0	17.857	29.413	**29.670**

3.2.2. Sequential parameter estimation

Various strategies have been applied to identify nonlinear chemical kinetic models (Vajda et al., 1989; Quaglio et al., 2019). In a sequential parameter estimation (SPE) strategy (Shahmohammadi and McAuley, 2019) parameters are decorrelated by manipulating the Fisher information matrix (FIM), an $N_\theta \times N_\theta$ symmetrical matrix. A non-invertible FIM indicates that the model is non-identifiable. FIM manipulation includes matrix reduction, single-value decomposition, or matrix transformation. In this work, we explore the leave-out (LO) procedure of sequential parameter estimation, an approach under matrix reduction that determines a subset of estimable parameters in a model and leaves the rest of the parameters at their nominal values (Thompson et al., 2010; Shahmohammadi and McAuley, 2019). The authors (Thompson et al., 2010; Shahmohammadi and McAuley, 2019) categorized the parameters fixed at their nominal values into three: (1) parameters that have small effects on the model prediction, (2) parameters that have correlated effects with more influential parameters and (3) parameters whose values are relatively well-known.

Knowledge about the process can help in categorizing the parameters. In the hydrogen borrowing scheme, the first chemical step is fully decoupled from other chemical steps. Benzyl alcohol, which is the reactant, does not participate in any parallel or subsequent steps. Concentration measurements of benzyl alcohol can thus be used to estimate the Arrhenius parameters for this chemical step. Other chemical steps such as the additive arylation and the reduction of the complex intermediate cannot be decoupled like this. Therefore, in the sequential PE, we will first estimate the values for the pre-exponential factor and the activation energy (θ_1, θ_2) for the oxidation of benzyl alcohol to benzyl aldehyde in a sub model $f_{Ox}(\theta_1, \theta_2)$ describing this reaction in PE 1. Subsequently, on estimating and fixing the parametric values of the oxidation sub model, we will estimate the values of the remaining parameters (i.e., $\theta_3, \theta_4, \ldots, \theta_P$) in the complete hydrogen borrowing model in PE 2. This sequential PE differs from a standard PE, which evaluates the full parameter set in a single stage. The sequential PE steps are listed in Algorithm 1.

Algorithm 1. : Sequential parameter estimation

Input: $\boldsymbol{f}(\dot{\boldsymbol{x}}(\tau), \boldsymbol{x}(\tau), \boldsymbol{\theta})$; $f_{Ox}(\dot{x}_{BnOH}(\tau), x_{BnOH}(\tau), \theta_1, \theta_2)$; $\mathcal{D} = [\boldsymbol{\varphi}, \boldsymbol{y}]$ /* $\mathcal{D}$ consists of experimental design setpoints $\boldsymbol{\varphi}$ and experimental data $\boldsymbol{y}$ */

Step 1. Compute θ_1, θ_2 by using $\mathcal{D}$ and f_{Ox} in the DAEs optimisation to express the log-likelihood function in Eq. (5); parameters $\theta_3, \theta_4, \ldots, \theta_P$ have negligible effects on f_{Ox}.

Step 2. Fix θ_1, θ_2 at the values obtained in (1) and compute $\theta_3, \theta_4, \ldots, \theta_P$ using $\mathcal{D}$ and $\boldsymbol{f}$ in the dynamic optimisation to express the log-likelihood function in Eq. (5).

Output: Full parameter set: $\boldsymbol{\theta}$ $[\theta_1, \theta_2, \theta_3, \theta_4, \ldots, \theta_P]$

Table 4
χ^2, AIC and Fisher information analyses for the six models indicating better model performance with the sequential PE than with the standard PE: values shown in red indicating unacceptable performance while models shown in green are acceptable.

	Model	Standard PE				Sequential PE			
		χ^2	χ^2_{ref}	AIC	FIM-D	χ^2	χ^2_{ref}	AIC	FIM-D
1	Model 1	79.67	60.48	24.73	0.00	26.49	60.48	10.38	397.00
2	Model 2	79.66	83.68	24.72	0.02	26.48	83.68	10.38	397.36
3	Model 3	55.75	92.81	24.07	0.00	23.01	92.81	12.54	0.00
4	Model 4	23.29	101.88	16.70	0.00	23.01	101.88	16.54	0.00
5	Model 5	23.29	113.15	16.70	0.00	23.01	113.15	16.55	0.00
6	Model 6	32.18	122.11	24.91	0.00	23.02	122.11	20.55	0.00

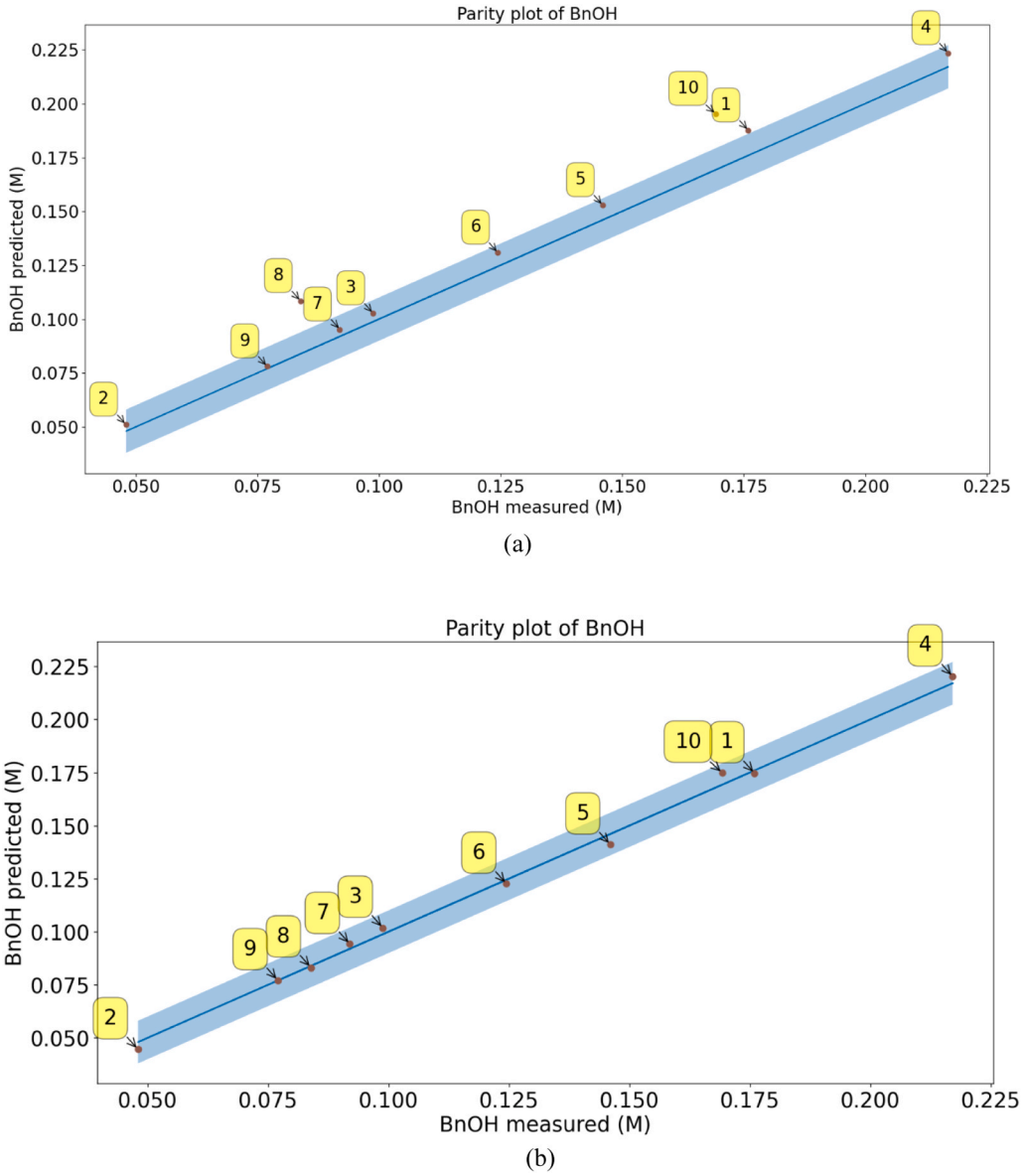

Fig. 5. Model 1 parity plots for the 10 experiments showing the results of sequential PE (b) are more accurate than the standard PE (a).

3.3. Model performance analysis

To investigate model reliability and the precision of the estimated parameters, we employ the following mathematical tools: χ^2 lack-of-fit test, Akaike information criterion (AIC) and a scalar measure of the Fisher information matrix.

3.3.1. The χ^2 lack-of-fit test

The χ^2 distribution is a statistic for testing the goodness-of-fit (or conversely, lack-of-fit) of a model to the data (Stewart et al., 1998). It assumes the residuals $(y_{sk} - \hat{y}_{sk})^2$ to be normally distributed and tests whether the model sum of residuals is below a reference value χ^2_{ref} estimated from the χ^2 distribution of the model degrees of freedom and the model confidence probability. The model degrees of freedom is given

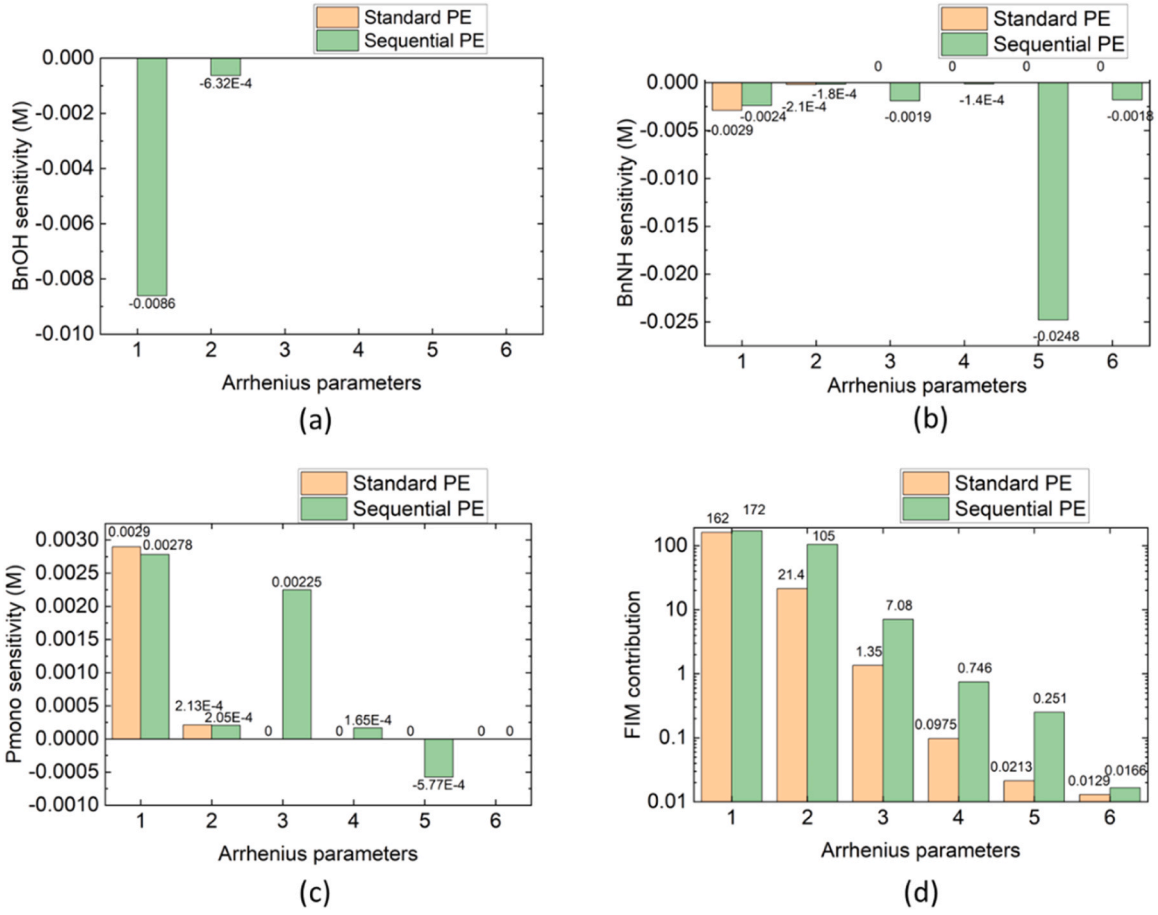

Fig. 6. Model 1 parameter sensitivity plots for responses BnOH (a), BnNH (b), Pmono (c) and the parameter contribution to FIM (d) with the Standard PE and sequential PE; Arrhenius parameters 1–6 denoting θ_1, θ_2, …, θ_6, respectively.

by $N_{\exp}N_y - N_\theta$ while the confidence probability is specified (a 0.95 confidence probability is used in this work). The chi-square value is defined as:

$$\hat{\chi}^2 = \sum_{s=1}^{N_{\exp}} \sum_{k=1}^{N_y} \frac{(y_{sk} - \hat{y}_{sk})^2}{\sigma_{kk}^2} \tag{11}$$

where y_{sk}, $\hat{y}_{sk}$ are the k^{th} entry of $\mathbf{y}$ at the s^{th} experiment of the measured and predicted response, respectively. Additionally, σ_{kk}^2 is the variance of the k^{th} measured response and the k^{th} diagonal entry of the measurement's variance-covariance. The $\hat{\chi}^2$ is compared with a tabulated reference value χ_{ref}^2, which is the inverse of the cumulative distribution function of χ^2 distribution at $1-\alpha$ confidence level (usually $\alpha = 0.05$ % or 0.01 %) with $N_{\exp}N_y - N_\theta$ degrees of freedom. The value of the $\hat{\chi}^2$ needs to be as small as possible and ideally less than χ_{ref}^2. Note that as the degrees of freedom increase, the reference value χ_{ref}^2 of the χ^2 distribution also increases, since the distribution spreads out to accommodate more sources of variability in the model (Casella and Berger, 2002).

3.3.2. Akaike information criterion

Akaike information criterion (AIC) (Akaike, 1975) is a criterion used to penalize against overfitting the data with a complex parametric model. AIC depends on the χ^2 value and the number of parameters. Assuming normally distributed error with a constant variance, the expression (Burnham and Anderson, 2004; Gkioulekas and Papageorgiou, 2018) is:

$$AIC = (N_{\exp} * N_y)\log\left(\hat{\chi}^2/(N_{\exp} * N_y)\right) + 2 * N_\theta \tag{12}$$

The model with the smallest AIC value is preferred as it represents the best trade-off between fitting model performance and complexity in terms of model parameters.

3.3.3. Fisher information matrix

The Fisher information matrix **H** corresponds to the inverse of the $N_\theta \times N_\theta$ posterior covariance matrix of parameter uncertainties **V**, which can be computed using the estimated parameters and expressed as (Galvanin et al., 2015):

$$\mathbf{V}(\hat{\theta}, \boldsymbol{\varphi}) = \left(\mathbf{H}(\hat{\theta}, \varphi) + \sum_0^{-1}\right)^{-1} \tag{13}$$

with

$$H_{ll'}(\hat{\theta}, \varphi) = \sum_S^{N_{\exp}} \sum_k^{N_y} \sum_{k'}^{N_y} S_{kk'} \frac{\partial \hat{y}_{sk}}{\partial \theta_l} \frac{\partial \hat{y}_{sk'}^T}{\partial \theta_{l'}} \tag{14}$$

$\boldsymbol{\Sigma_0}$ is the preliminary approximation of the variance-covariance matrix of the parameters, which contains the initial information on parametric uncertainty; $s_{kk'}$ is the kk' element of the $N_y \times N_y$ inverse of the variance-covariance matrix of the measurement errors $\boldsymbol{\Sigma}_\mathbf{y}$; $\frac{\partial \hat{y}_{sk}}{\partial \theta_l}$ is the parameter sensitivity of $\hat{y}_{sk}$ the k^{th} entry of $\hat{\mathbf{y}}$ at the s^{th} experiment with respect to θ_l. As a square matrix, the determinant of **H** denoted as $|\mathbf{H}|$ can be calculated and used as a scalar measure of the Fisher information matrix.

The matrix **H** is approximately the Hessian matrix of the objective function in Eq. (5) and must be positive-definite as a sufficient condition for a local minimum (Bard, 1974). Thus, for **H** being non-singular its

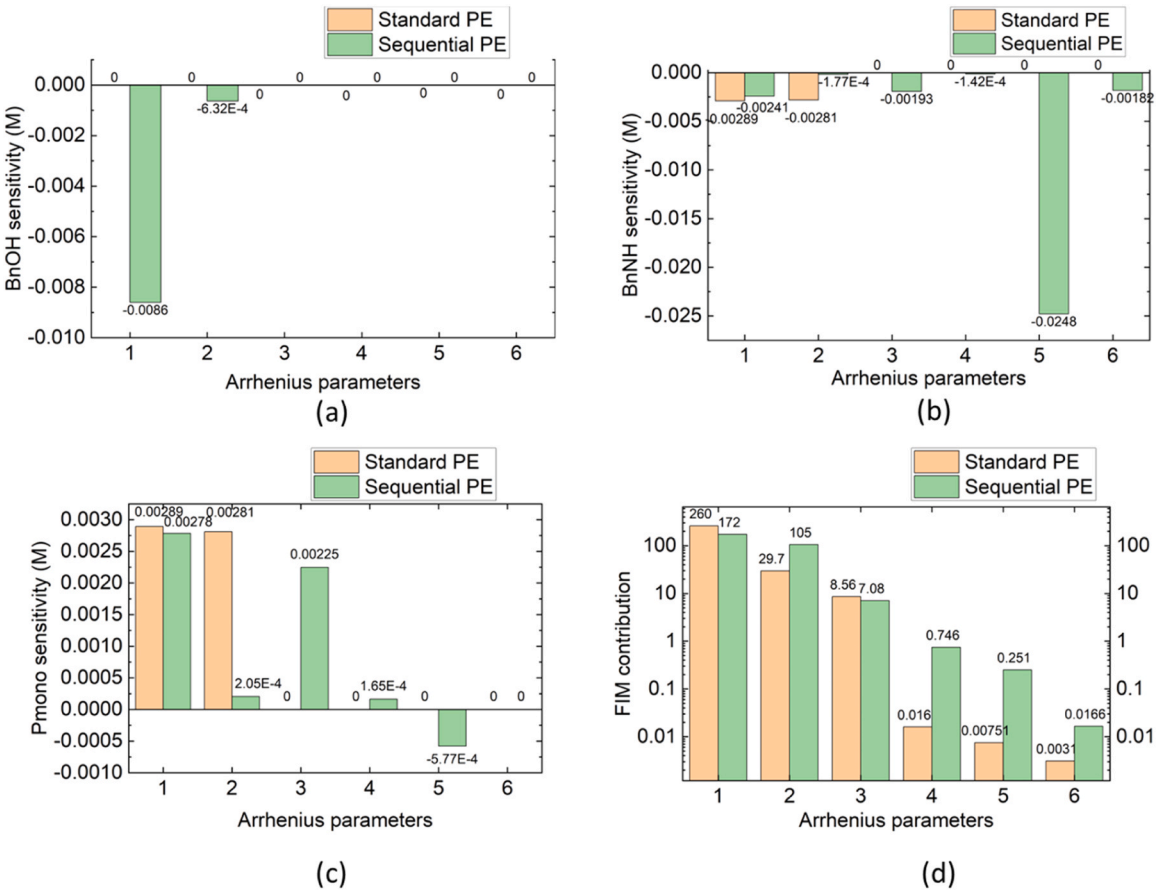

Fig. 7. Model 2 parameter sensitivity plots for responses BnOH (a), BnNH (b), Pmono (c) and the parameter contribution to FIM (d) with the standard PE and sequential PE; Arrhenius parameters 1–6 denoting θ_1, θ_2, …, θ_6, respectively.

Table 5
Condition numbers of the FIM obtained for Models 1–6 using the standard and sequential parameter estimation techniques: values in red are deemed unacceptable (i.e., value below the threshold of $5.\bullet 10^4$) while those in green acceptable.

Model	*Condition number* $\kappa = \frac{\lambda_{max}}{\lambda_{min}}$	
	Standard PE	Sequential PE
Model 1	$7.97 \bullet 10^7$	$1.02 \bullet 10^4$
Model 2	$8.93 \bullet 10^4$	$1.02 \bullet 10^4$
Model 3	$8.07 \bullet 10^{21}$	$1.37 \bullet 10^9$
Model 4	$3.90 \bullet 10^6$	$4.15 \bullet 10^7$
Model 5	$3.77 \bullet 10^{21}$	$4.15 \bullet 10^7$
Model 6	$1.40 \bullet 10^7$	$6.46 \bullet 10^{11}$

determinant used in this work as an identifiability metric must be greater than zero. In numerical computations, the condition number of a matrix, which is the ratio of largest to smallest eigenvalues, can be used to check the matrix singularity. Via the eigen decomposition, **H** can be expressed as (Stroud and Dexter, 2020):

$$\mathbf{H} = \mathbf{U}\mathbf{\Lambda}\mathbf{U}^{\mathrm{T}} \tag{15}$$

where **U** is the unitary matrix whose columns are the normalized eigenvectors of **H** while **Λ** is the diagonal matrix of the eigenvalues. Then the condition number is:

$$\kappa = \frac{\lambda_{max}}{\lambda_{min}} \tag{16}$$

For numerical convergence of the objective function to a solution, Bard reported a maximum value of 10^5 for the condition number (Bard, 1974).

Table 6
Parameter values and their respective *t*-values calculated using the sequential parameter estimation at $T_{ref} = 225$ °C.

	$\boldsymbol{\theta}$ $k_i(\mathrm{M}^{-1}\mathrm{s}^{-1})$/ E_{ai}(kJ/mol)	θ_1 k_1	θ_2 E_{a1}	θ_3 k_2	θ_4 E_{a2}	θ_5 k_3	θ_6 E_{a3}
Model 1	Parameter values	1.4E−4	110	0.02	9.95E−8	4.7E−4	37.1
	t-value	48.6	63.3	0.2	5.8E−8	37.5	21.3
	(*tref* (95 %)= 2.0)						
Model 2	Parameter values	0.14	110	0.02	9.96E−8	4.7E−4	37.1
	t-value	21.8	63.9	0.2	5.8E−8	37.8	21.3
	(*tref* (95 %)= 2.0)						

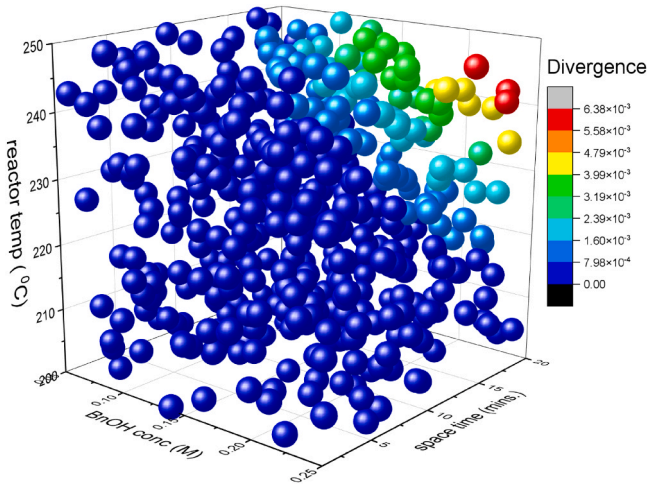

Fig. 8. Divergence region based on the Buzzi-Ferraris criterion in the experimental design for discriminating between Models 1 and 2.

3.4. MBDoE module

The MBDoE module employs one or more identifiable candidate kinetic models, i.e. models characterised by a non-singular Fisher information matrix, to design optimal experimental conditions resulting in the most informative data. With two or more models satisfying preliminary parameter testing, we employ MBDoE for model discrimination to select the best model among them. This technique computes experiments that maximize the joint divergence among the models, which is a linear combination of the pairwise divergences J_{ij}. The joint divergence $J_{1,2,3,\dots}$ is (Box and Hill, 1967):

$$J_{1,2,3,\dots} = \sum_{i \neq j} L^i L^i J_{ij} \tag{17}$$

where subscript 1, 2, 3 counts the number of satisfactory models, L^i is the likelihood of model i. The pairwise divergence is given as (Bard, 1974):

$$J_{i,j} = \int \left[p^i(\boldsymbol{x}) - p^j(\boldsymbol{x})\right] \log \left[p^i(\boldsymbol{x})/p^j(\boldsymbol{x})\right] d\boldsymbol{x} \tag{18}$$

where p^i is the model i probability density function.

These expressions are not computationally tractable. Computationally tractable forms that have been employed include the Hunter-Reiner and Buzzi-Ferrari criteria (Buzzi-Ferraris et al., 1990; Olofsson et al., 2019). For the Hunter-Reiner criteria, the expression is (Olofsson et al., 2019; Hunter and Reiner, 1965):

$$\sum_{i=1}^{M-1} \sum_{j=i+1}^{M} \left[\left(\boldsymbol{y}_{n+1}{}^i - \boldsymbol{y}_{n+1}{}^j\right)^T \boldsymbol{Q} \left(\boldsymbol{y}_{n+1}{}^i - \boldsymbol{y}_{n+1}{}^j\right) \right] \tag{19}$$

where $\boldsymbol{Q}$ is a diagonal scaling matrix.

This criterion neither accounts for parameter uncertainty nor does it require experimental error for the divergence criterion for multiple models when designing experiments for discrimination. For the Buzzi-Ferrari criteria, the expression is (Buzzi-Ferraris et al., 1990):

$$\sum_{i=1}^{M-1} \sum_{j=i+1}^{M} \left[\left(\boldsymbol{y}_{n+1}{}^i - \boldsymbol{y}_{n+1}{}^j\right)^T \boldsymbol{\Sigma}_{ij}{}^{-1} \left(\boldsymbol{y}_{n+1}{}^i - \boldsymbol{y}_{n+1}{}^j\right) + trace(2\boldsymbol{\Sigma}_y \boldsymbol{\Sigma}_{ij}{}^{-1}) \right] \tag{20}$$

where

$$\boldsymbol{\Sigma}_{ij} = 2\boldsymbol{\Sigma}_y + \boldsymbol{\Sigma}_i + \boldsymbol{\Sigma}_j \tag{21}$$

$\boldsymbol{\Sigma}_i(\mathrm{u}_{\mathrm{exp}+1})$ is the model i posterior prediction covariance matrix for the marginal posterior experiment:

$$\boldsymbol{\Sigma}_i(\mathrm{u}_{\mathrm{exp}+1}) = \mathbf{G}_i \boldsymbol{\Theta}_i \quad {}^{-1}\mathbf{G}_i{}^T \tag{22}$$

$$\mathbf{G}_i\left(\mathrm{u}_{\mathrm{exp}+1}\right) = \begin{bmatrix} \frac{\partial x_1}{\partial \theta_1} & \frac{\partial x_1}{\partial \theta_2} & \cdots & \frac{\partial x_1}{\partial \theta_P} \\ \frac{\partial x_2}{\partial \theta_1} & \frac{\partial x_2}{\partial \theta_2} & \cdots & \frac{\partial x_2}{\partial \theta_P} \\ \vdots & \vdots & \ddots & \vdots \\ \frac{\partial x_n}{\partial \theta_1} & \frac{\partial x_n}{\partial \theta_2} & \cdots & \frac{\partial x_n}{\partial \theta_P} \end{bmatrix} \tag{23}$$

This criterion accounts for parameter uncertainty and experimental error when designing experiments for discrimination.

Following experimentation at the designed condition for model discrimination and re-estimating the model parameters with updated experimental data, statistical analysis can be re-employed on the recalibrated models to test their predictions and decide on the best model. The predictions have associated χ^2 values that can be calculated and used to obtain the maximum likelihood L_i for each model with the expression:

$$L_i = \left.\frac{1}{\chi^2}\right|_i \tag{24}$$

Bard expressed (Bard, 1974) the values of the maximum likelihood for two models in a probability ratio L_1/L_2, which can then be used as a criterion to decide on the best model. The probability ratio must be larger (or lower) than a particular value M (or its inverse $1/M$), calculated using the expected confidence in the results as:

$$M = \frac{(1-\alpha_2)}{\alpha_1} \tag{25}$$

where α_1 is the maximum error permitted in Model 1 from the true model while α_2 is the maximum error permitted in Model 2 from the true model. For instance, where the error permitted in each alternative model must not exceed 5 %, $M = (1 - 0.05)/0.05 = 19$. The probability ratio must be greater than 19 to select Model 1 as the best model (or less than $1/19$ to select Model 2 as the best model). The decision is inconclusive otherwise. For more than two alternative models, the probability fraction p_f can be used as:

$$p_f = \frac{L_i}{\sum_{i=1}^{N_m} L_i} \tag{26}$$

where N_m is the number of models.

4. Results and discussions

In this section, we analyse the parameter estimation techniques on the developed models and subject identifiable models to model discrimination.

4.1. Parameter estimation analysis

In this section, we discuss the performances of the developed hydrogen borrowing kinetic models whose Arrhenius parameters have been estimated using the standard full-set parameter estimation and sequential parameter estimation techniques. The experimental design space $\boldsymbol{\varphi}$ for the experimental decision variables in the hydrogen borrowing reaction between benzyl amine and benzyl alcohol consists of an equivalent inlet concentration of benzyl alcohol (to react with a constant inlet concentration of benzyl amine), space time and reactor temperature, as reported in Table 2. Within this design space, 10 experiments were designed using the Latin hypercube sampling (LHS) and then executed in the LabBot subsystem. Resulting experimental

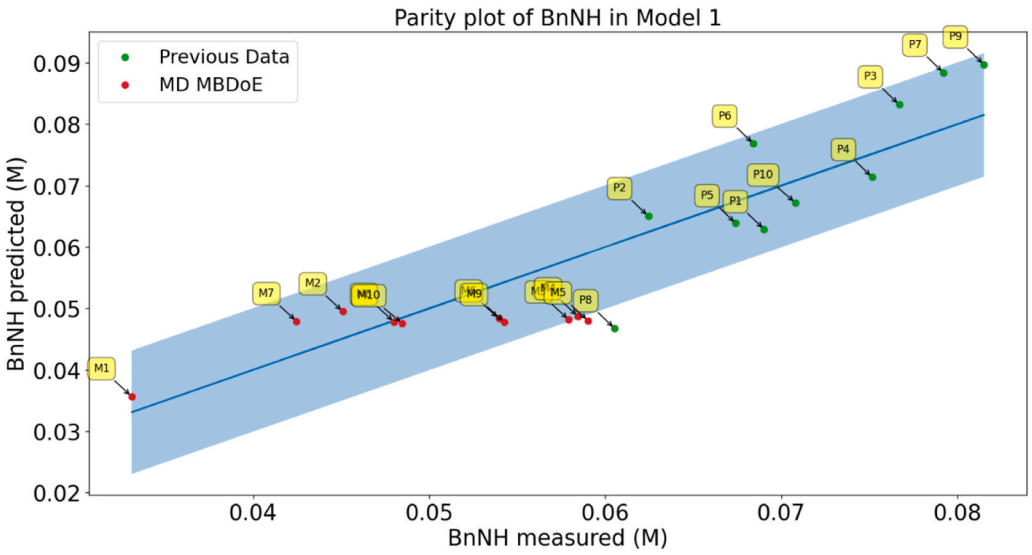

(a)

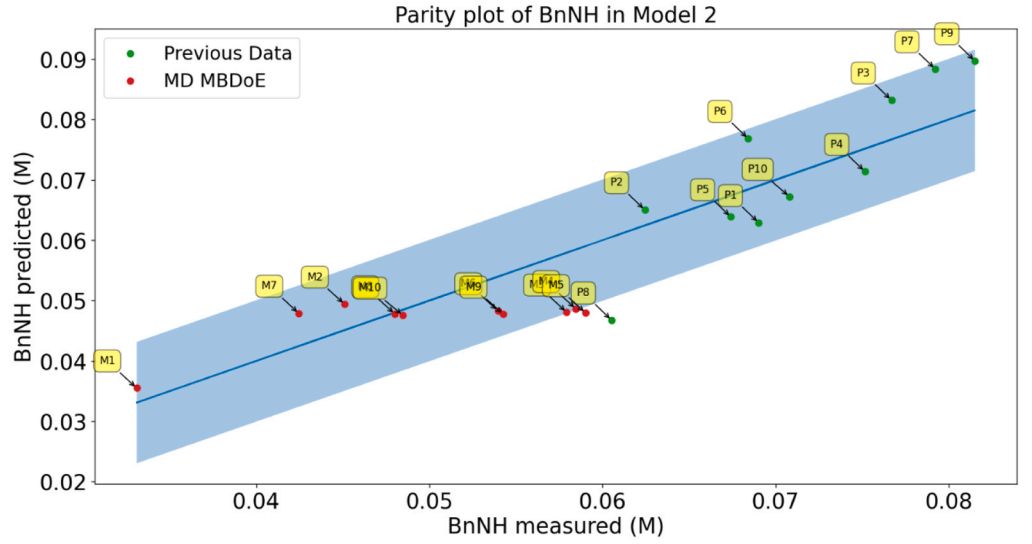

(b)

Fig. 9. Updated parity plot of benzyl amine (BnNH) showing the previous experimental points and the in-silico model discrimination points for Model 1 (A) and Model 2 (B) showing similar distributions.

measurements were employed for parameter estimation. These 10 experiments are described by the horizontal steps shown in Fig. 4 while Table 3 shows their corresponding outlet measurements from the LabBot subsystem with products diphenylamine and triphenylamine called Pmono and Pbis, respectively.

Table 3 shows zero for the PBis concentration because the amount produced in these 10 experiments were too low to be measured by the LabBot subsystem. This species was however detected in other experiments, not reported in this article, during the preliminary stage to familiarize the LabBot setup with the synthesis and determine the experimental design space, hence the inclusion of the second cycle in the overall mechanism for the hydrogen borrowing reaction between benzyl amine and benzyl alcohol. Conversions of benzyl amine and benzyl alcohol are also reported, benzyl amine recording higher conversion in all the experiments. These conversion data cannot be explained with only the hydrogen borrowing scheme which requires 2 moles of benzyl alcohol for every mole of benzyl amine to complete the 2 cycles reported in Section 2: each of the 2 cycles requires benzyl alcohol while only the first cycle requires benzyl amine. To explain this unusual, higher than expected conversion, we assume that in addition to reacting in the hydrogen scheme, benzylamine decomposes to another substance, named X, which could be alkylbenzene, cyclohexanone or benzyl aldehyde (DTIC Defense Technical Information Center, 1970). Decomposition of benzylamine to one or a combination of these compounds has been reported in literature (DTIC Defense Technical Information Center, 1970; Lewis, 2004; NCBI National Center for Biotechnology Information, 2023). Thus, we modified the hydrogen scheme as reported in Fig. 3 and derived the 6 kinetic models reported in Table 1.

Table 4 shows values of χ^2, AIC and FIM-D for the six candidate models with their parameters estimated using the standard and sequential PE techniques. The χ^2 values resulting from the sequential PE are lower than those obtained from a standard PE. As the value of χ^2 relates directly with maximizing the negative log-likelihood function, the SPE estimated the parameter values more efficiently than the standard PE. To illustrate the optimization efficiency, Model 1 parity plots, which graphically describe the χ^2 term and model accuracy for the two parameter estimation approaches, are shown in Fig. 5. Model

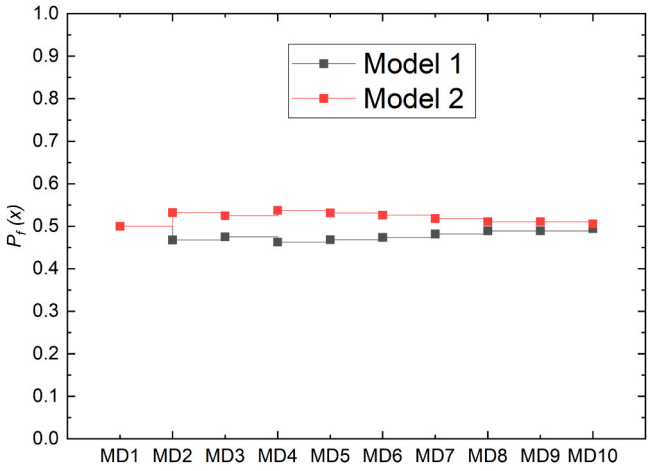

Fig. 10. the χ^2 probabilities of Models 1 and 2 for model discrimination (MD) in 10 experiments.

predictions with sequential parameter estimates are more accurate than those with standard full-set parameter estimates. The sequential technique, by decorrelating the parameters, can obtain parametric values that minimize the sum of residuals better than the standard full-set technique.

Further, the χ^2 data adequacy test is satisfied with the sequential PE implemented on the six models; the six models can therefore represent the data adequately. The standard PE using the χ^2 test, however, rejects Model 1, the simplest model, as inadequate in describing the experimental data. This model also has the second highest AIC value from standard PE. Conversely, Model 1 along with Model 2 has the lowest AIC value from sequential PE because in this approach the number of parameters term in Eq. (12) dominates over the χ^2 term.

Further, from Table 4, the standard PE rejects all the six models as unidentifiable and their resulting FIM determinant values are all zero, suggesting practical non-identifiability. On the other hand, when SPE is used, Models 1 and 2 become identifiable, i.e., they exhibit non-singular Fisher information matrix. FIM entries are derived from parameter sensitivities as shown in Eq. (14). Fig. 6 presents the parameter sensitivity analysis for Model 1 from both parameter estimation methods. Subfigures A, B and C display the sensitivity of BnOH, BnNH and Pmono, respectively, to variations in individual model parameters. Subfigure D summarizes the overall contribution of each parameter to the FIM, highlighting which parameters most influence model identifiability and which responses are most informative.

The parameter sensitivities of Standard PE for Model 1 shown in Fig. 6A, B and C, reveal that the three responses are insensitive to changes in parameters θ_3 and θ_4, which are the Arrhenius parameters for the arylation step involving BnNH and BnCHO; these insensitive responses yield values approaching zeros as row/column entries in the $N_\theta \times N_\theta$ Fisher information matrix, hence resulting in a determinant value approaching zero. For the sequential PE, on the other hand, the responses are sensitive to changes in parameters. While reactant BnOH responds to changes in only θ_1 and θ_2, reactant BnNH and product Pmono respond to changes in all the parameters. Consequently, the FIM entries are non-zero values, yielding a non-singular and invertible

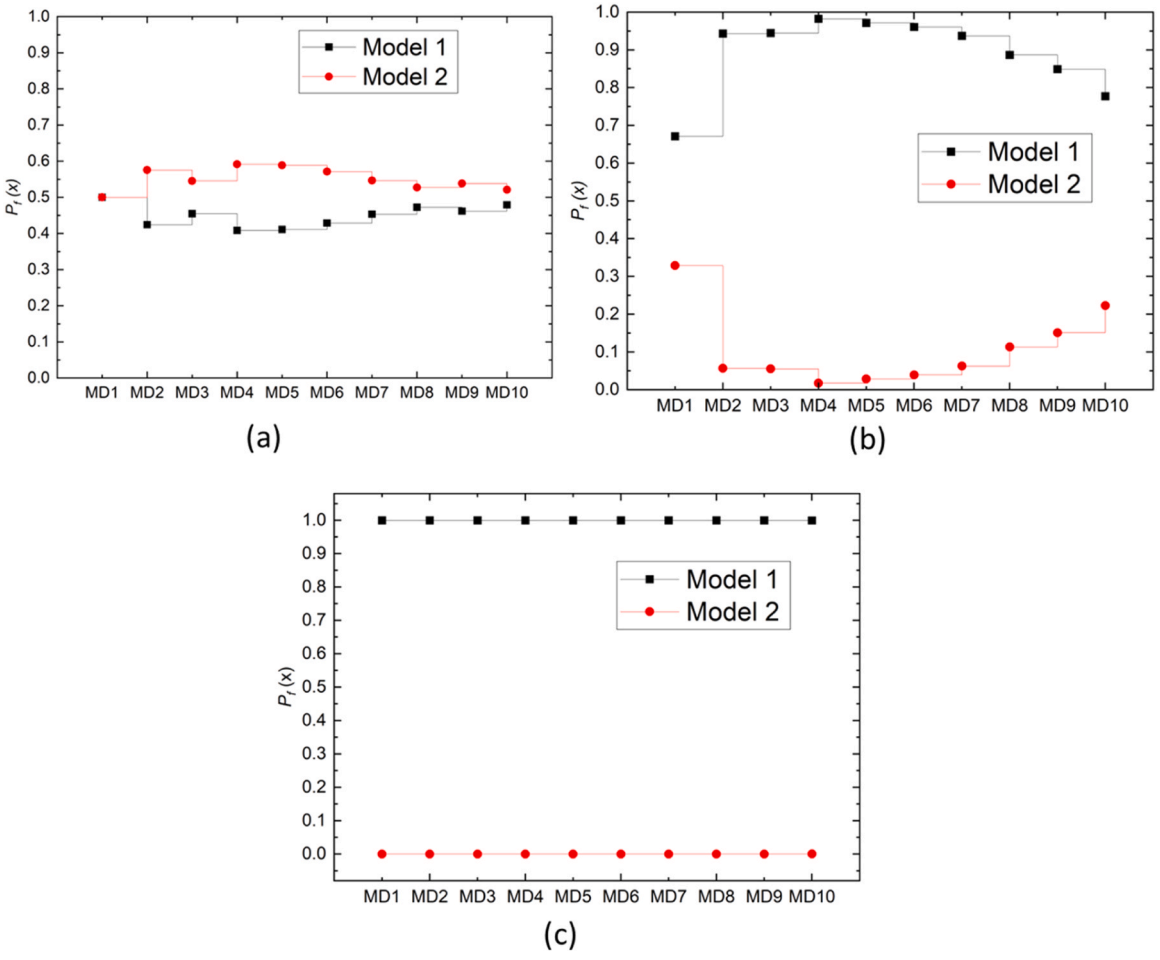

Fig. 11. Model discrimination experiments (MD) via in-silico studies between Models 1 and 2 with catalyst decrease of (a) 1 %, (b) 2 % and (c) 3 %.

matrix.

Model 2 exhibits a similar behavior with standard and sequential PEs (see Fig. 7). In the former, changing parameters θ_3 and θ_4 does not have a noticeable effect on any of the three measured concentrations (BnNH, BnCHO and Pmono), resulting in rows/columns of entries with values approaching zeros. In the latter, changing the parameters has at least an effect on one of the three measured concentrations. Matrices with zero rows/columns are not full-rank and their condition numbers are very large ($\kappa \geq 10^5$), as illustrated in Table 5, which reports the condition numbers of the FIM estimated from the two parameter estimation techniques for the six models.

Kinetic models developed without accounting for the degradation of benzylamine are reported in Appendix 1 in the ES1. These models failed the χ^2 lack-of-fit test as their χ^2 values calculated from both parameter estimation techniques are larger than the reference values. We refer to the ESI for details.

4.2. Model-based design of experiment for model discrimination

MBDoE for model discrimination can be applied to Models 1 and 2, both of which contain identifiable parameters estimated using the sequential parameter technique. The estimated parameter values and their associated uncertainties are presented in Table 6, where statistical significance is evaluated using *t*-test values. The formula for calculating the *t*-values is provided in Appendix 2 of the ESI. For each model, two of the six parameters exhibited *t*-values below the reference threshold, indicating substantial uncertainty in the estimates. Notably, these parameters are associated with the arylation step in the hydrogen borrowing reaction mechanism.

Despite this uncertainty, both models remain statistically identifiable and are therefore suitable for in-silico MBDoE-based model discrimination, to design new experiments aimed at maximizing divergence in model responses (see Eq. (18)).

Fig. 8 shows the region in the experimental design space obtained via in-silico data for model discrimination between Models 1 and 2 using the Buzzi-Ferraris criterion (Eq. (20)). The Hunter-Reiner criterion for model discrimination (Eq. (19)) yielded identical divergence region (see Appendix 3 in the ESI).

To test the potential for model discrimination between Models 1 and 2, we assumed Model 1 as the true model and employ in-silico data to obtain the probability of discriminating between the two most promising kinetic models. To generate the in-silico data, we first designed an experiment in the most divergent point within the experimental design space as illustrated in Fig. 8, then simulated the designed experiment using Model 1 and finally introduced random noise (with zero mean and 5×10^{-3} standard deviation) to the Model 1 predictions for BnNH, BnOH and Pmono. In line with the hydrogen borrowing chemical synthesis discussed in Section 2, the model predictions of other reactive chemical species (*BnCHO* and MH_2 in Table 1) gave nearly zero concentration, while the metal catalyst remained constant at $10^{-4}M$ (0.1 % of the inlet concentration of BnNH). With the in-silico data added to 10 prior experimental data, we recalibrated Models 1 and 2 and analysed the two models using χ^2 probability, derived by combining Eqs. (24) and (25). To pass the discrimination test, the probabilities of the two models should diverge with new in-silico data, the assumed true model (i.e., Model 1) exceeding 0.95 probability while Model 2 was below 0.05. Via this procedure, 10 model discrimination experiments were sequentially designed and performed in-silico. Fig. 9 shows an updated parity plot for benzylamine comprising the 10 previous experimental data (P points) and the 10 optimally designed in-silico model discrimination data (MD points). The corresponding model discrimination χ^2 probabilities of Models 1 and 2 are shown in Fig. 10.

As shown, the model probabilities do not diverge but remain close to 0.5. We simulated for 50 more model discrimination experiments and obtained no divergence in information between the two models. We can therefore infer that Models 1 and 2 are not distinguishable.

Consequently, we exploit the model structural differences: Model 1 being zeroth order with respect to the catalyst amount while Model 2 being first order (see Table 1), assuming the catalyst amount as a new experimental design variable ($\boldsymbol{u}$), which can be set from information about catalyst structure and composition (Auepattana-aumrung et al., 2020). Results from further in-silico model discrimination studies, assuming a decrease of 1, 2 and 3 % in catalyst amount are shown in Fig. 11. At 1 % catalyst decrease, Model 1 (the true model) still behaves similarly as Model 2 (the rival model) with the discrimination probability, which is in favor of the rival model, in the 10 in-silico model discrimination experiments ranging between 0.5 and 0.6. The two models cannot be distinguished as a threshold probability of 0.95 must be reached or exceeded for model distinguishability. At 2 % catalyst decrease, the discrimination probability, which is in favor of the true model, started at about 0.7, and then increased briefly, exceeding the threshold probability of 0.95 at the model discrimination experiment #4. Thereafter, the discrimination decreased to about 0.75 at the model discrimination experiment #10 as the 2 % catalyst decrease could not sustain divergence in the two model predictions and clear model distinguishability at 0.95. However, at 3 % catalyst decrease, the discrimination probability exceeded 0.99 in the 10 discrimination experiments providing clear model discrimination. A catalyst decrease of 3 % or larger (also investigated in-silico) is therefore required to ensure model distinguishability

5. Conclusions

In this work, using previously reported mechanistic theory, we have developed kinetic models for the hydrogen borrowing reaction, a common synthetic step employed in the pharmaceutical industry for drug discovery. The synthesis was conducted in a smart flow reactor controlled via a cloud-based system composed of modules for preliminary design of experiments, kinetic model development, parameter estimation and model-based design of experiments. In a preliminary model development stage, data for measurable species in the LabBot obtained from a statistical DoEs were used to identify suitable hydrogen borrowing mechanisms and derive candidate kinetic models. Candidate models were proposed, from the simplest model, only based on observed measurable species, to the most complex model, comprising all chemical species including intermediate species involved in the detailed reaction mechanism. Two approaches were compared to estimate the kinetic parameters of the candidate kinetic models: (i) a standard full-set nonlinear parameter estimation (PE) and (ii) a sequential parameter estimation (SPE) where only subsets of identifiable parameters are sequentially estimated. A Fisher information matrix analysis was used to screen out unidentifiable candidate models and showed that a standard PE would fail to identify any suitable model from the set of candidate models while SPE could identify two identifiable models (Model 1 and Model 2) and found them adequate to describe the hydrogen borrowing reaction data generated by the LabBot.

The two identifiable models were therefore employed in the MBDoE techniques for in-silico model discrimination studies comparing different model discrimination criteria, namely the Buzzi-Ferraris criterion and the Hunter Reiner criterion. Although the Buzzi-Ferraris design criterion identified a region of discrimination in the experimental design space, further analysis showed that model discrimination between the two models was not possible based on current data, which is limited by what species can be monitored. However, exploiting the model structural differences in-silico, the catalyst amount was identified as a key model discrimination driver to exploit in the experiments, with a decrease of at least 3 % in catalyst amount ensuring complete distinguishability (i.e. discrimination probability higher than 0.99) between Model 1, employed as the ground truth, and Model 2. Future validation experiments will be needed to confirm the impact of catalyst decrease on model discrimination and hence the adequacy of Model 2 in

representing reaction kinetics in the hydrogen borrowing system.

CRediT authorship contribution statement

Chamberlain Thomas W.: Writing – review & editing, Supervision, Resources, Funding acquisition, Conceptualization. **Ricardo Labes:** Data curation. **Emmanuel Agunloye:** Writing – review & editing, Writing – original draft, Visualization, Methodology, Investigation, Formal analysis, Data curation, Conceptualization. **Federico Galvanin:** Writing – review & editing, Supervision, Methodology, Funding acquisition, Conceptualization. **Richard A. Bourne:** Supervision, Resources, Project administration, Funding acquisition, Conceptualization. **Frans L. Muller:** Supervision, Resources, Funding acquisition, Conceptualization.

Declaration of Competing Interest

The authors declare that they have no known competing financial interests or personal relationships that could have appeared to influence the work reported in this paper.

Acknowledgments

The project has received funding from EPSRC (EP/R032807/1 and EP/X024016/1). The support is gratefully acknowledged.

Appendix A. Supporting information

Supplementary data associated with this article can be found in the online version at doi:10.1016/j.cherd.2025.09.005.

References

AGI (Ansys Government Initiative), 2024. Introduction to IPOPT: A tutorial for downloading, installing, and using IPOPT, ⟨https://help.agi.com/stk/LinkedDocuments/IPOPTreference.pdf⟩.

Agunloye, E., Petsagkourakis, P., Yusuf, M., Labes, R., Chamberlain, T., Muller, F.L., Bourne, R.A., Galvanin, F., 2024. Automated kinetic model identification via cloud services using model-based design of experiments. React. Chem. Eng. https://doi.org/10.1039/D4RE00047A.

Akaike, H., 1975. A new look at the statistical model identification. December 1974 IEEE Trans. Autom. Control 19 (6), 716–723. https://doi.org/10.1109/TAC.1974.1100705.

Andersson, J.A.E., Gillis, J., Horn, G., Rawlings, J.B., Diehl, M., 2019. CasADi: a software framework for nonlinear optimization and optimal control. Math. Prog. Comp. 11, 1–36. https://doi.org/10.1007/s12532-018-0139-4.

Auepattana-aumrung, C., Márquez, V., Wannakao, S., Jongsomjit, B., Panpranot, J., Praserthdam, P., 2020. Role of al in Na-ZSM-5 zeolite structure on catalyst stability in butene cracking reaction. Sci. Rep. 10 (13643), 2020. https://doi.org/10.1038/s41598-020-70568-z.

Bard, Y. Academic Press 1974.

Biegler, L., 2010. Nonlinear programming - concepts, algorithms, and applications to chemical processes, computer science. MOSSIAM Ser. Optim. 2010.

Box, G.E.P., Draper, N.R., 1987. Empirical Model-Building and Response Surfaces. Wiley, New York.

Box, G.E.P., Hill, W.G., 1967. Discrimination among mechanistic models. Technometrics 9, 57–71. https://doi.org/10.2307/1266318.

Burnham, K.P., Anderson, D.R., 2004. Multimodel inference: understanding AIC and BIC in model selection (PDF). Sociol. Methods Res. 33, 261–304. https://doi.org/10.1177/0049124104268644.

Buzzi-Ferraris, G., Forzatti, P., Paolo, C., 1990. An improved version of a sequential design criterion for discriminating among rival multiresponse models. ISSN 0009-2509 Chem. Eng. Sci. 45 (2), 477–481. https://doi.org/10.1016/0009-2509(90)87034-P.

Bynum, M.L., Hackebeil, G.A., Hart, W.E., Laird, C.D., Nicholson, B.L., Siirola, J.D., Watson, J.-P., Woodruff, D.L., 2021. Pyomo – optimization modeling in python, 3rd edition. Springe Optim. Appl. https://doi.org/10.1007/978-3-030-68928-5.

Caliński, T., Kageyama, S., 2000. Block designs: a randomization approach, volume i: analysis. In: Lecture Notes in Statistics, 150. Springer-Verlag, New York.

CasADi, 2024. Welcome to CasADi Documentation, ⟨https://web.casadi.org/docs/⟩.

Casella, G., Berger, R.L., 2002. Statistical inference, second ed. Chapman and Hall/CRC, Imprint. https://doi.org/10.1201/9781003456285.

Chatterjee, S., Moore, C.M.V., Nasr, M.M., 2017. An overview of the role of mathematical models in implementation of quality by design paradigm for drug development and manufacture. In: Reklaitis, G.V., Seymour, C., García-Munoz, S. (Eds.), Comprehensive Quality by Design for Pharmaceutical Product Development and Manufacture. John Wiley & Sons Inc, New York (NY; USA), pp. 9–24. https://doi.org/10.1002/9781119356189.ch2.

Collins, P.C., 2018. Chemical engineering and the culmination of quality by design in pharmaceuticals. AIChE J. 64, 1502–1510. https://doi.org/10.1002/aic.16154.

Destro, F., Barolo, M., 2022. A review on the modernization of pharmaceutical development and manufacturing – trends, perspectives, and the role of mathematical modelling. ISSN 0378-5173 Int. J. Pharm. 620 (2022), 121715. https://doi.org/10.1016/j.ijpharm.2022.121715.

DTIC (Defense Technical Information Center), 1970. DTIC AD0879619: Autoxidation of Biologically Active Amines.

Fisher, A.C., Kamga, M.H., Agarabi, C., Brorson, K., Lee, S.L., Yoon, S., 2019. The current scientific and regulatory landscape in advancing integrated continuous biopharmaceutical manufacturing. Trends Biotechnol. 37, 253–267. https://doi.org/10.1016/j.tibtech.2018.08.008.

Franceschini, G., Macchietto, S., 2008. Model-based design of experiments for parameter precision: state of the art. Chem. Eng. Sci. 63 (19), 4846–4872. https://doi.org/10.1016/j.ces.2007.11.034.

Galvanin, F., Cao, E., Al-Rifai, N., Gavriilidis, A., Dua, V., 2015. Model-based design of experiments for the identification of kinetic models in microreactor platforms, Editor (s): krist V. Gernaey, jakob K. Huusom, rafiqul gani. In: Computer Aided Chemical Engineering, 37. Elsevier. https://doi.org/10.1016/B978-0-444-63578-5.50049-9.

Gkioulekas, I., Papageorgiou, L.G., 2018. Piecewise regression through the akaike information criterion using mathematical programming. IFACPaperOnLine 51 (15), 730–735. https://doi.org/10.1016/j.ifacol.2018.09.168 (ISSN 2405-8963).

Huang, M., Li, Y., Lan, X.B., Liu, J., Zhao, C., Liu, Y., Ke, Z., 2021. Ruthenium(II) complexes with *n*-heterocyclic carbene-phosphine ligands for the *n*-alkylation of amines with alcohols. Org. Biomol. Chem. 19 (15), 3451–3461. https://doi.org/10.1039/d1ob00362c. PMID: 33899900.

Hunter, W.G., Reiner, A.M., 1965. Designs for discriminating between two rival models. Technometrics 7 (3), 307–323. https://doi.org/10.2307/1266591.

Karimi, A., Majlesi, M., Rafieian-Kopaei, M., 2015. Herbal versus synthetic drugs; beliefs and facts. J. Nephropharmacol. 4 (1), 27–30. PMID: 28197471; PMCID: PMC5297475.

Kaylor, A., 2025. Advanced pharmaceutical manufacturing is modernizing drug production, improving efficiency and enhancing scalability with innovative technologies like 3D printing and continuous manufacturing. ⟨https://www.techtarget.com/PharmaLifeSciences/feature/Understanding-advanced-pharma-manufacturing-technology⟩, accessed 18/06/2025.

Kent, J.A., Bommaraju, T.V., Barnicki, S.D., 2016. Handbook of Industrial Chemistry and Biotechnology, thirteenth ed. Springer. https://doi.org/10.1007/978-3-319-52287-6.

Lee, S.L., O'Connor, T.F., Yang, X., Cruz, C.N., Chatterjee, S., Madurawe, R.D., Moore, C.M.V., Yu, L.X., Woodcock, J., 2015. Modernizing pharmaceutical manufacturing: from batch to continuous production. J. Pharm. Innov. 10, 191–199. https://doi.org/10.1007/s12247-015-9215-8.

Leonard, J., Blacker, A.J., Marsden, S.P., et al., 2015. A survey of the borrowing hydrogen approach to the synthesis of some pharmaceutically relevant intermediates (3 more authors). Org. Process Res. Dev. 19 (10), 1400–1410. ISSN 1083-6160 https://doi.org/10.1021/acs.oprd.5b00199.

Lewis, R.J.Sr, 2004. Sax's Dangerous Properties of Industrial Materials, eleventh ed. Wiley-Interscience, Wiley & Sons, Inc., Hoboken, NJ, p. 399. https://doi.org/10.1002/0471701343 (ed). (ed).

NASEM (National Academies of Sciences, Engineering, and Medicine), 2024. Innovations in Pharmaceutical Manufacturing on the Horizon: Technical Challenges, Regulatory Issues, and Recommendations. National Academies Press (US). https://doi.org/10.17226/26009.

NCBI (National Center for Biotechnology Information) 2023. PubChem Compound Summary for CID 7504, Benzylamine. Retrieved August 23, 2023 from ⟨https://pubchem.ncbi.nlm.nih.gov/compound/Benzylamine⟩.

Olofsson, S., Hebing, L., Niedenführ, S., Deisenroth, M.P., Misener, R., 2019. GPdoemd: a python package for design of experiments for model discrimination. Comp. Chem. Eng. 125, 54–70. https://doi.org/10.1016/j.compchemeng.2019.03.010.

Powner, E.T., Yalcinkaya, F., 1995. From basic sensors to intelligent sensors: definitions and examples (December). Sens. Rev. 15 (4), 19–22. https://doi.org/10.1108/02602289510102327.

Quaglio, M., Waldron, C., Pankajakshan, A., Cao, E., Gavriilidis, A., Fraga, E.S., Galvanin, F., 2019. 2019. An online reparametrisation approach for robust parameter estimation in automated model identification platforms. Comput. Chem. Eng. 124, 270–284. https://doi.org/10.1016/j.compchemeng.2019.01.010.

Reed-Berendt, B.G., Latham, D.E., Dambatta, M.B., Morrill, L.C., 2021. Borrowing hydrogen for organic synthesis. ACS Cent. Sci. 7 (4), 570–585. https://doi.org/10.1021/acscentsci.1c00125.

Rossi, C.V., 2022. A comparative investment analysis of batch versus continuous pharmaceutical manufacturing technologies, 2022 J. Pharm. Innov. 17 (4), 1373–1391. https://doi.org/10.1007/s12247-021-09612-y.

Schwaab, M., Lemos, L.P., Pinto, J.C., 2008. Optimum reference temperature for reparameterization of the arrhenius equation. Part 2: problems involving multiple reparameterizations. ISSN 0009-2509 Chem. Eng. Sci. 63 (11), 2895–2906. https://doi.org/10.1016/j.ces.2008.03.010.

Shahmohammadi, A., McAuley, K.B., 2019. Sequential model-based A-optimal design of experiments when the fisher information matrix is noninvertible. Ind. Eng. Chem. Res. 58 (3), 1244–1261. https://doi.org/10.1021/acs.iecr.8b03047.

Srinath, S., Gunawan, R., 2010. Parameter identifiability of Power-Law biochemical system models. J. Biotechnol. 149, 132. https://doi.org/10.1016/j.jbiotec.2010.02.019.

Stewart, W.E., Shon, Y., Box, G.E.P., 1998. Discrimination and goodness of fit of multiresponse mechanistic models. AlChE J. 44 (1998), 1404–1412. https://doi.org/10.1002/aic.690440618.

Stroud, K.A., Dexter, J.B., 2020. Advanced Engineering Mathematics, eighth ed. Bloomsbury Publishing. ISBN 9781352010275.

Thompson, D.E., McAuley, K.B., McLellan, P.J., 2010. Design of optimal sequential experiments to improve model predictions from a polyethylene molecular weight distribution model, 2010 Macromol. React. Eng. 4 (1), 73–85. https://doi.org/10.1002/mren.200900033.

Vajda, S., Rabitz, H., Walter, E., Lecourtier, Y., 1989. Qualitative and quantitative identifiability analysis of nonlinear chemical kinetic models. Chem. Eng. Commun. 83 (1), 191–219. https://doi.org/10.1080/00986448908940662.

Wächter, A., Biegler, L., 2006. On the implementation of a primal-dual interior point filter line search algorithm for large-scale nonlinear programming. Math. Program 106 (1), 25–57 (2006).

Waldron, C., Pankajakshan, A., Quaglio, M., Cao, E., Galvanin, F., Gavriilidis, A., 2019. Closed-Loop Model-Based design of experiments for kinetic model discrimination and parameter estimation: benzoic acid esterification on a heterogeneous catalyst. Ind. Eng. Chem. Res. 58 (49), 22165–22177. https://doi.org/10.1021/acs.iecr.9b04089.

Wichrowski, N.J., Fisher, A.C., Arden, N.S., Yang, X., 2020. An overview of drug substance manufacturing processes. AAPS PharmSciTech 21 (271), 2020. https://doi.org/10.1208/s12249-020-01806-w.

Yu, L.X., Amidon, G., Khan, M.A., Hoag, S.W., Polli, J., Raju, G.K., Woodcock, J., 2014. Understanding pharmaceutical quality by design. AAPS J. 16, 771–783.

Yu, L.X., Raw, A., Wu, L., Capacci-Daniel, C., Zhang, Y., Rosencrance, S., 2019. FDA's new pharmaceutical quality initiative: knowledge-aided assessment & structured applications. Int. J. Pharm. X 1. https://doi.org/10.1016/j.ijpx.2019.100010.

Yuangyai, C., Nembhard, H.B., 2008–2010. Design of experiments: a key to innovation in nanotechnology. in Emerging Nanotechnologies for Manufacturing. Copyright © 2009 by Academic Press.

Yue, H., Brown, M., Knowles, J., Wang, H., Broomhead, D.S., Kell, D.B., 2006. Insights into the behaviour of systems biology models from dynamic sensitivity and identifiability analysis: a case study of an NF-KB signalling pathway. Mol. BioSyst. 2, 640. https://doi.org/10.1039/b609442b.